X-ray Crystal Structures of HMG-CoA Synthase from *Enterococcus faecalis* and a Complex with Its Second Substrate/Inhibitor Acetoacetyl-CoA[†,‡]

C. Nicklaus Steussy,[§] Anthony A. Vartia,[||] John W. Burgner, II,[§] Autumn Sutherlin,[⊥] Victor W. Rodwell,[@] and Cynthia V. Stauffacher*[,§,#]

Department of Biological Sciences, Purdue University, West Lafayette, Indiana 47907, Department of Pharmaceutical Chemistry, University of Kansas, Lawrence, Kansas 66047, Department of Chemistry, Abilene Christian University, Abilene, Texas 79699, Department of Biochemistry, Purdue University, West Lafayette, Indiana 47907, and Purdue Cancer Center, Purdue University, West Lafayette, Indiana 47907

Received July 27, 2005; Revised Manuscript Received August 4, 2005

ABSTRACT: Biosynthesis of the isoprenoid precursor, isopentenyl diphosphate, is a critical function in all independently living organisms. There are two major pathways for this synthesis, the non-mevalonate pathway found in most eubacteria and the mevalonate pathway found in animal cells and a number of pathogenic bacteria. An early step in this pathway is the condensation of acetyl-CoA and acetoacetyl-CoA into HMG-CoA, catalyzed by the enzyme HMG-CoA synthase. To explore the possibility of a small molecule inhibitor of the enzyme functioning as a non-cell wall antibiotic, the structure of HMG-CoA synthase from *Enterococcus faecalis* (MVAS) was determined by selenomethionine MAD phasing to 2.4 Å and the enzyme complexed with its second substrate, acetoacetyl-CoA, to 1.9 Å. These structures show that HMG-CoA synthase from *Enterococcus* is a member of the family of thiolase fold enzymes and, while similar to the recently published HMG-CoA synthase structures from *Staphylococcus aureus*, exhibit significant differences in the structure of the C-terminal domain. The acetoacetyl-CoA binary structure demonstrates reduced coenzyme A and acetoacetate covalently bound to the active site cysteine through a thioester bond. This is consistent with the kinetics of the reaction that have shown acetoacetyl-CoA to be a potent inhibitor of the overall reaction, and provides a starting point in the search for a small molecule inhibitor.

Isoprenoids are molecules essential to all known independent life forms. Built up from the common building block of the phosphorylated five-carbon compound isopentenyl diphosphate (IPP),[1] the isoprenoids encompass more than 30 000 different biological molecules with diverse function (*1*). IPP is synthesized via two distinct and independent pathways (*2*). In most eubacteria, algae, and plants, IPP is synthesized in the non-mevalonate or GAP pathway that begins with the condensation of pyruvate and glyceraldehyde 3-phosphate (GAP) (*3*). In mammals, yeast, and some pathogenic Gram-positive bacteria, the production of IPP starts with the condensation of acetyl-CoA and acetoacetyl-CoA, catalyzed by HMG-CoA synthase, to produce 3-hydroxy-3-methylglutaryl-CoA (HMG-CoA).

HMG-CoA synthase (EC 2.3.3.10) is a 42 kDa protein found in a wide range of organisms from bacteria to mammals (*2*). Phylogenetic analysis and X-ray crystal structures of the enzyme from *Staphylococcus* and those presented here show that this enzyme is a member of the thiolase superfamily, which includes enzymes important in lipid metabolism and involved in the biosynthesis of various polyketide compounds (*4*, *5*). The active form of HMG-CoA synthase in *Enterococcus* appears to be a homodimer, although there is no evidence for cooperativity between active sites from steady-state kinetics experiments (*6*). In cells from higher eukaryotes, there are two isoforms of HMG-CoA synthase encoded by two separate genes (*7*). The cytosolic isoform in mammals (*8*) is involved in the mevalonate pathway and is under the control of sterol regulatory binding elements (SREBPs), which reflects feedback control by cholesterol and other sterols (*8*, *9*). In contrast, the mitochondrial isoform is central to ketogenesis (*10*, *11*) and is under the control of the peroxisome proliferator regulatory element (PPRE) (*12*), which enhances transcription of the mitochondrial enzyme during fasting.

[†] This work was supported by grants from the National Institutes of Health, Heart, Lung and Blood Institute, awarded to C.V.S. (HL52115) and to V.W.R. (HL47113), as well as an American Heart Association grant awarded to V.W.R. (0150503N). Support of the core facilities for macromolecular crystallography is provided in part through a grant to the Purdue Cancer Center from the National Cancer Institute (NCI CA23568) and by the Markey Center for Structural Biology, Purdue University.

[‡] The coordinates and structure factors for the two structures of HMG-CoA synthase presented here have been deposited in the Protein Database, as entries 1X9E for the native enzyme and 1YSL for the complex with acetoacetyl-CoA.

* To whom correspondence should be addressed. Telephone: (765) 494-4937. Fax: (765) 496-1189. E-mail: cstauffa@purdue.edu.

[§] Department of Biological Sciences, Purdue University.

[||] University of Kansas.

[⊥] Abilene Christian University.

[@] Department of Biochemistry, Purdue University.

[#] Purdue Cancer Center, Purdue University.

[1] Abbreviations: CoA, coenzyme A; IPP, isopentenyl diphosphate; MVAS, HMG-CoA synthase from *Enterococcus faecalis*; APS, The Advanced Photon Source at Argonne National Laboratory; MAD, multiwavelength anomalous diffraction.

10.1021/bi051487x CCC: $30.25 © 2005 American Chemical Society
Published on Web 10/05/2005

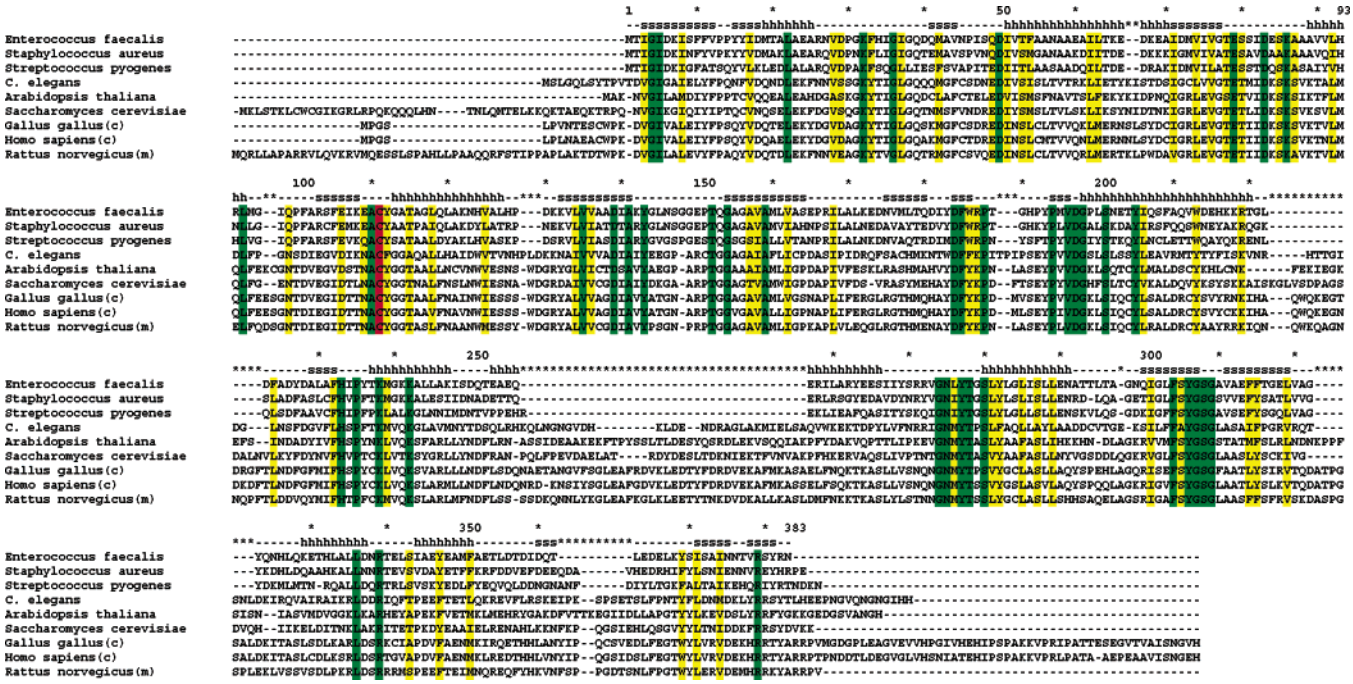

FIGURE 1: Sequence alignment of HMG-CoA synthases. This figure shows an alignment of amino acid sequences of HMG-CoA synthases (EC 2.3.3.10) from organisms across a wide phylogenetic range. Identical residues are highlighted in green and similar residues in yellow. The sequences were drawn from the Swiss-Prot protein knowledgebase (http://us.expasy.org/swissprot), and when the subcellular location was annotated, it is indicated with a (c) for cytoplasmic or an (m) for mitochondrial. The catalytic cysteine (residue 111 in *E. faecalis*) is colored red. The alignment of the sequences was conducted with the ClustalW algorithm at the SDSC Biology Workbench (http://workbench.sdsc.edu). The sequences used were as follows: *Arabidopsis thaliana* (P54873), *S. cerevisiae* (baker's yeast, P54839), *G. gallus* (chicken) cytoplasmic isoform (P23228), *Homo sapiens* (human) cytoplasmic isoform (Q01581), *Rattus norvegicus* (Rat) mitochondrial isoform (P22791), *Caenorhabditis elegans* (nematode, P54871), *S. aureus* (bacteria, Q9FD87), *E. faecalis* (bacteria, Q9FD71), and *S. pyogenes* (bacteria, Q8P1D3). The secondary structure of the residues is indicated in a row of text above the sequence for *E. faecalis* with h indicating a helix, s a strand, and − a loop region. A larger version of this figure is available as Supporting Information.

A comparison of the sequences of HMG-CoA synthase demonstrates that this enzyme has diverged across the phylogenetic branches (Figure 1 and Supporting Information). The overall level of identity across different phyla is only 13% (see Figure 1), concentrated in short stretches of residues presumably conserved for essential structural and catalytic functions. The sequence alignment in Figure 1 demonstrates these conserved regions and also illustrates the differences in the domain structure between the two HMG-CoA synthase isoforms. The bacterial enzymes are the shortest, retaining only the essential catalytic components. The mammalian mitochondrial enzyme has an N-terminal 40-amino acid extension containing the signal sequence that directs the compartmentalization of this isoform. In contrast, the cytosolic isoform in mammals has a 50-amino acid extension at the C-terminus of unknown function.

The reaction catalyzed by HMG-CoA synthase is the irreversible condensation of acetyl-CoA with acetoacetyl-CoA to produce HMG-CoA (Figure 2). The first step in the reaction involves the formation of an enzyme acetyl-CoA binary complex, followed by the transfer of the acetyl group from the CoA thioester to a cysteine residue on the enzyme, forming a thioester acyl−enzyme intermediate (Rx1 in Figure 2). After the dissociation of now reduced CoA, the second substrate, acetoacetyl-CoA, binds the enzyme (Rx2). The next step involves the formation of a carbanion by removal of a proton from the methyl of the acetylcysteine. The activated acetylcysteine then undergoes a Claisen-like condensation (Rx3) with the γ-carbon of the acetoacetyl-CoA ligand which forms the HMG-CoA while retaining the

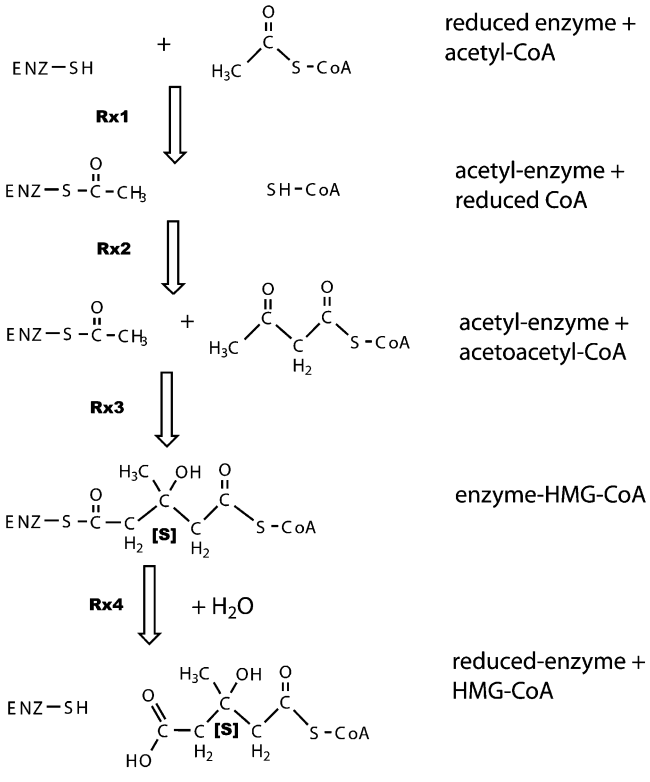

FIGURE 2: Mechanism of HMG-CoA synthase. Figure adapted from ref *19*.

thioester bond to the enzyme. Hydrolysis of this bond results in free HMG-CoA, which is the substrate for subsequent reactions in the pathway (*12*, *13*). It is of note that the K_m

Table 1: HMG-CoA Synthase Mutants and Their Effects[a]

E. faecalis	*G. gallus*	mutation	V_{max}	%	K_m (μM)	%	ref
n/a[b]	WT	n/a[b]	4.400	100	290	100	*18*
E79	E95	E95A	0.000	0	n/a[b]	n/a[b]	*19*
C111	C129	C129S	0.000	0	n/a[b]	n/a[b]	*18*
Y143	Y163	Y163L	0.780	18	200	69	*23*
D184	D203	D203A	0.003	<1	37	13	*20*
F185	F204	F204L	0.012	<1	260	90	*23*
Y205	Y225	Y225L	1.660	38	125	43	*23*
H233	H264	H264A	0.220	5	122	42	*22*
		H264N	0.130	3	172	59	*22*
Y277	Y346	Y346L	0.380	9	604	208	*23*
Y306	Y376	Y376L	0.440	10	604	208	*23*

[a] Kinetic parameters of selected mutations of avian HMG-CoA synthase taken from the indicated references. The equivalent residue in *E. faecalis* is listed in the first column. The experiments were carried out with saturating amounts of acetoacetyl-CoA using a spectrophotometric assay. [b] Not applicable or not available.

for acetyl-CoA is in the millimolar range, while acetoacetyl-CoA in anything more than micromolar amounts is a potent inhibitor of the overall reaction (*14*, *15*).

Extensive mutagenesis experiments with HMG-CoA synthase from *Gallus gallus* have identified residues that are important to the enzyme mechanism. Early studies detected the presence of an essential cysteine residue, which serves as the acceptor of the acetyl group in the covalent enzyme intermediate (*16*, *17*). The presence of a modified acetylcysteine was directly confirmed by detection of the tetrahedral intermediate (*18*). Mutation studies of conserved acidic residues have identified a number of critical residues which modulate either the formation of the acetylcysteine or the subsequent condensation reaction (*19*−*21*). Evaluation of other invariant residues identified a single required histidine, which has been implicated in both of these steps in the reaction mechanism (*22*). Several aromatic residues were implicated as being part of the active site, including an absolutely required phenylalanine residue (*23*). A summary of a subset of these mutants of HMG-CoA synthases important to our structural interpretation is given in Table 1.

Recently, a number of common human pathogens, including *Enterococcus faecalis*, *Streptococcus pneumoniae*, and *Staphylococcus aureus*, have been shown to utilize the mevalonate pathway for biosynthesis of IPP, with null mutants of pathway enzymes dependent on external mevalonate for growth (*24*, *25*). This raises the possibility that a targeted inhibitor of the mevalonate pathway would be an antibacterial *specific* for these pathogens that are common causes of infection following trauma or surgical procedures. Such an agent would have a significant therapeutic advantage over the commonly used broad-spectrum antibiotics in that their antibacterial action would be specifically targeted at the pathogenic bacteria. This would leave the normal commensal bacterial population intact, discouraging fungal overgrowth or colonization with multi-antibiotic resistant bacteria. It would thus be an ideal agent to employ in hospitalized, immune-compromised patients, such as burn victims or cancer patients undergoing chemotherapy. In addition, the bacteriocidal mechanism of such an inhibitor would be unique and so potent against the methicillin resistant pathogens that are becoming more common (*26*).

To better understand the mechanism of catalysis and to create the groundwork for a rational drug design program directed against the mevalonate pathway in pathogens, we elected to determine the structure of an HMG-CoA synthase from the pathogen *E. faecalis* in its native form and in complex with the potent second-substrate inhibitor acetoacetyl-CoA.

METHODS

HMG-CoA synthase from *E. faecalis* (MVAS) was cloned, expressed, and purified as described previously (*6*). This construct produces approximately 30 mg of N-terminal six-His-tagged protein per liter of culture. The protein was purified using a nickel−NTA (Invitrogen) resin column to single-band purity as evaluated by SDS−PAGE. Initial crystallization conditions were defined with the assistance of the robotic crystallization project at the Hauptman-Woodward Institute (2004) and suggestions from N. Campobasso (Glaxo SmithKline, personal communication). These initial findings were optimized using a sitting drop technique to final crystallization conditions of 2.4 M ammonium sulfate in 100 mM MES (pH 6.8) with a protein concentration of approximately 10 mg/mL.

Crystals of MVAS grew at 20 °C in 7−10 days. Initial crystals were bundles of thin rods that were improved by microseeding in crystallization drops with the protein concentration adjusted to less than 10 mg/mL. The best crystals grew as bundles of rods, optimally measuring 200 μm × 40 μm × 40 μm. Single-crystal fragments were broken off from these bundles, cryoprotected with a stepwise introduction of 30% (v/v) glycerol in the crystallization buffer, and flash-frozen in a nitrogen gas stream at 100 K. The diffraction potential of these crystals was screened on a local R-Axis IV^{++} area detector mounted on a Rigaku RU-200 rotating anode X-ray source. The best crystals were stored in liquid nitrogen for experimental data collection at the Advanced Photon Source (APS) at Argonne National Laboratory (Argonne, IL).

Initial data from a native MVAS crystal were collected at the Industrial Macromolecular Crystallography Association (IMCA) beamline 17ID at APS. This crystal diffracted to 2.4 Å in an *I*222 space group with the following cell dimensions: $a = 105.4$ Å, $b = 109.8$ Å, and $c = 141.5$ Å. However, the data exhibited marked deterioration during the experiment and were not used in the final structure determination.

Selenomethionine-labeled HMG-CoA synthase was produced by transferring the MVAS expression plasmid to methionine auxotrophic *Escherichia coli* cells (B834 from Novagen). Protein expression was induced in vitamin- and ion-supplemented minimal media in which selenomethionine was substituted for methionine (*27*). The resulting selenomethionine-derivatized protein was purified initially as for the native protein. An anion exchange chromatography step utilizing a MonoQ column (purchased from Pharmacia Corp.) and elution with a sodium chloride gradient from 60 to 500 mM at pH 7.0 was added to the protocol to further purify the protein. Crystallization conditions for SeMet MVAS were virtually identical to those for the native protein and produced similar bundles of rods that diffracted to 2.4 Å resolution.

Table 2 summarizes the results of a three-wavelength MAD experiment with the selenomethionine-derivatized MVAS crystals conducted at the BioCARS beamline 14ID-B

Table 2: Data Collection and Refinement Statistics

	inflection	peak	remote (native)	acetoacetyl-enzyme
location	APS 14ID	APS 14ID	APS 14ID	APS 14-BM-C
energy (keV)	12.660	12.662	12.960	13.775
space group	*I*222	*I*222	*I*222	*I*222
cell dimensions				
a (Å)	105.3	105.4	105.3	105.3
b (Å)	109.8	109.8	109.8	109.0
c (Å)	141.3	141.5	141.5	140.8
resolution (Å)[a]	30−2.40 (2.49−2.40)	30−2.50 (2.40−2.50)	30−2.40 (2.49−2.40)	28−1.90 (1.97−1.90)
no. of unique reflections	61243	54396	61488	123107
completeness[a]	99.1 (99.0)	99.1 (99.5)	99.0 (98.6)	99.7 (99.9)
redundancy (*x*-fold)[a]	4.3 (3.9)	4.3 (4.0)	4.3 (3.8)	2.5 (2.5)
$I/\sigma I$[a]	12.8 (3.7)	14.1 (3.3)	13.2 (3.4)	21.4 (3.8)
R_{merge}[a,b]	12.5 (40.5)	12.1 (44.8)	12.1 (43.5)	8.7 (42.0)
no. of selenium sites	19/20	19/20	19/20	
refinement				
Wilson *B* (Å^2)			12.3	16.3
mean *B* (Å^2)			16.5	23.7
no. of atoms			5972	5972
no. of residues			766	766
no. of waters			170	521
R_{work}/R_{free}[c]			0.235/0.254	0.183/0.206
rmsd for bonds (Å)			0.015	0.008
rmsd for angles (deg)			1.5	1.3
Protein Data Bank entry			1X9E	1YSL

[a] Data from the lowest-resolution bin shown in parentheses. [b] $R_{merge} = \sum_{hkl}\sum|I - \langle I\rangle|/\sum(I)\sum_{hkl}\sum|I - \langle I\rangle|/\sum(I)$, where I is the intensity. [c] $R = \sum||F_{obs}| - |F_{calc}|/\sum|F_{obs}|$. R_{free} is a control monitoring reflections left out of refinement.

at APS. To minimize the effect of crystal deterioration observed during the native data collection, the STRATEGY module of HKL2000 (*28*) was used in planning a minimal data collection using an inverse beam geometry to observe the anomalous reflections. The resulting data sets were 99% complete and approximately 4-fold redundant overall with a mosaic spread of 0.6°. The data were reduced and scaled using DENZO and SCALEPACK (*28*) in an *I*222 space group with unit cell dimensions closely similar to those of the native enzyme crystals. Matthews calculations (*29*) suggested two molecules in the asymmetric unit and a self-rotation Patterson map showed a large noncrystallographic peak with a κ of 180°. The data were truncated at 2.4 Å based on an $I/\sigma I$ cutoff of 3.0, resulting in an overall R_{merge} of 12%. Local scaling and initial phasing were accomplished by SOLVE (*30*) which located 19 of 20 selenium sites expected from a dimer in the asymmetric unit. Solvent flattening (*31*) with NCS averaging was followed by initial model building using the automated build feature of the companion program RESOLVE, version 2.02 (*32*), which produced the initial $2F_o - F_c$ electron density map seen in Figure 3. This model was corrected and expanded with iterative rounds of interactive graphics model building and solvent molecule placement in O (*33*) and refinement in CNS (*34*). Final rounds of refinement were done with Refmac5 (*35*), part of the CCP4 suite (*36*), resulting in an overall R_{work}/R_{free} of 0.235/0.254. The final monomer model contains all 383 amino acids of MVAS and one cis peptide, as well as 170 solvent molecules and four sulfate ions. Table 2 lists the final statistics for the data collection and refinement. Coordinates for the structure have been deposited in the Protein Data Bank as entry 1X9E.

The structure of MVAS complexed with acetoacetyl-CoA was pursued using a cocrystallization protocol. Briefly, native protein from the initial expression vector was purified to single-band purity as evaluated on an SDS−PAGE gel using a nickel−NATA column. Because of the oxidation of the

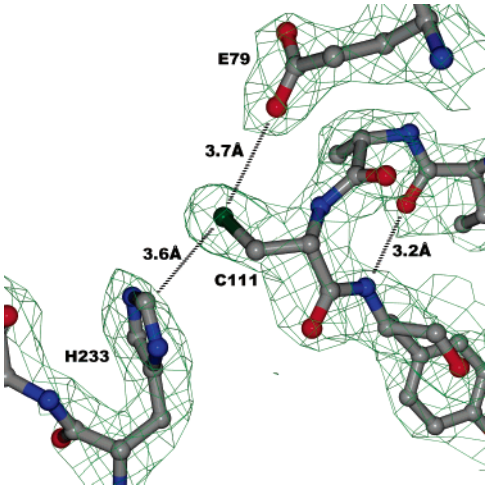

FIGURE 3: Electron density of the catalytic loop. This figure depicts the central active site residues with the associated electron density from the structure of native MVAS. The β-turn of the catalytic loop is shown with the pivotal hydrogen bond between the carbonyl of Ala110 and the amide of Tyr112. Distances between the γS of Cys111 and the known important active site residues, His233 and Glu79, are also illustrated. The density is an unrefined $2F_o - F_c$ map from the initial phasing and solvent flattening in RESOLVE (*32*), shown at a 1.5σ (relative) level.

catalytic cysteine seen in the binary structure from *Staphylococcus* (*37*), the MonoQ anion exchange step was modified to use a very shallow gradient elution with 1.0 M NaCl and care was taken to have reducing agents present at all stages of the purification and crystallization. The crystallization conditions were identical to the ones for the native protein except that 1 μL of acetoacetyl-CoA at a concentration of 5 mM was added to each 6 μL crystallization drop at the outset of the experiment. After equilibration with the reservoir solution, the final concentration of acetoacetyl-CoA in the crystallization drop of 2−3 mM is approximately a 10-fold molar excess with respect to the protein (10 mg/mL or 0.21

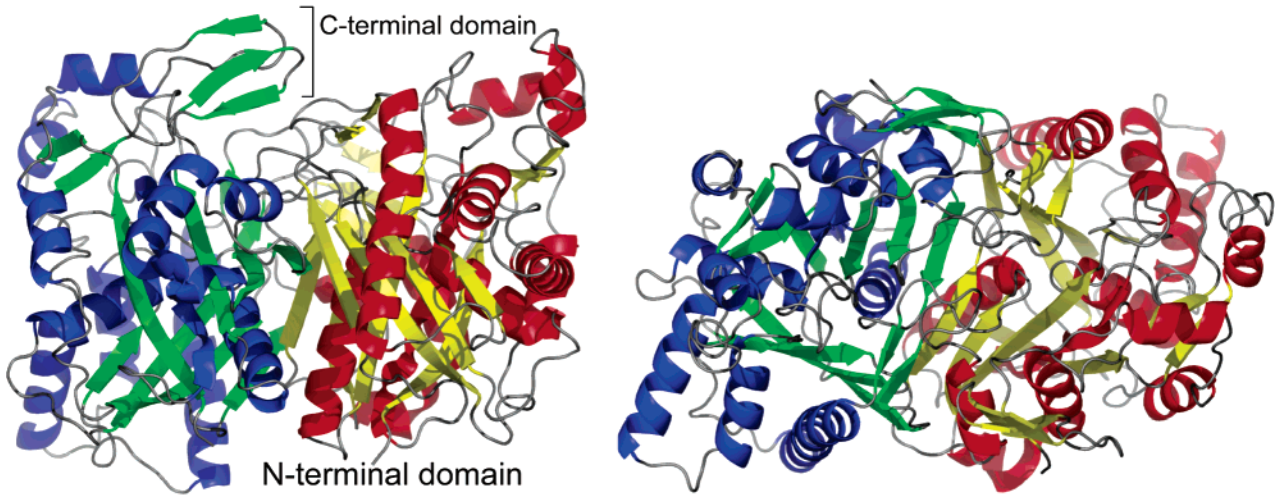

FIGURE 4: Ribbon illustration of the structure of the MVAS dimer. The ribbon cartoons of the secondary structural elements in MVAS dimer are colored such that monomer A is blue and green and monomer B is yellow and red. The identification of the residues forming these elements was conducted with DSSP (*45*) and visual review with interactive graphics in O (*33*). The left-hand view emphasizes the extended 10-strand β-sheet that bridges the two molecules at the center of the dimer as well as the small C-terminal β-sheet of the blue and green monomer, located at the top left. The right-hand panel shows the dimer rotated about a horizontal axis by 90°.

mM) and 200 times the apparent K_m (10 μM) of acetoacetyl-CoA for the synthetic reaction (*6*).

The crystals of the MVAS−acetoacetyl-CoA complex grew in the usual bundles in a week and did not require the seeding technique needed to grow the diffraction size native crystals. The acetoacetyl-CoA crystals were cryoprotected and screened for diffraction in the same fashion as the selenomethionine crystals. Diffraction data were collected at the Advanced Photon Source, beamline 14-BM-C, using a fixed 0.9 Å X-ray beam of exceptional brilliance. A redundant data set was collected and processed to a resolution of 1.9 Å using DENZO and SCALEPACK (*28*) which demonstrated the symmetry of the crystal was again *I*222 with cell dimensions virtually identical to those of the native and selenomethionine crystals. Initial phasing was done with the native MVAS model, and the first maps clearly exhibited $F_o - F_c$ density in the active site of the B monomer, but not in the A monomer. Given the difference between the monomers and the unmodeled density in the active site, subsequent refinement was undertaken without the use of noncrystallographic symmetry averaging between the monomers to prevent averaging out the differences. Interactive model correction in O and careful least-squares refinement with CNS were undertaken as with the native structure model. It became clear that the cysteine in the A active site was oxidized as seen in the recently published structure of staphylococcal MVAS (*37*). However, the B active site had extensive density continuous with the cysteine that was easily fit with an acetoacetate in a thioester linkage with the sulfur. Additional density in this active site was identified as the reduced CoA-SH in an extended conformation. These ligands were modeled in CNS and their occupancies adjusted to give temperature factors in the same range as those of the side chains of the model, following the technique used by Theisen et al. (*38*) in modeling the multiple contents found in the active site of their staphylococcal MVAS structure. Data collection and refinement statistics for MVAS complexed with acetoacetyl-CoA are presented in Table 2. The final model and structure factors have been deposited in the Protein Data Bank as entry 1YSL.

RESULTS AND DISCUSSION

N-Terminal Domain. Our experimentally phased structure of HMG-CoA synthase (MVAS) from the human pathogen *E. faecalis* shows the N-terminal domain of the protein to have a classic thiolase fold (*4*) with an HMG-CoA synthase specific C-terminal domain comprising residues 319−383. The characteristics of the N-terminal domain of MVAS in common with other thiolases include its association as a compact homodimer. The dimer interface is extensive, encompassing 18% of the accessible monomer surface area, and demonstrating a close interaction between structural elements from one monomer with the active site of the other. The large globular domain (residues 1−318) has mixed $\alpha-\beta$ secondary structural elements dominated by two β-sheets that envelop the two central α-helices (Figure 4). These two β-sheets each have two additional α-helices located on the exterior surface of the monomer, imparting the classic $\alpha-\beta-\alpha-\beta-\alpha$ five-layer appearance. The conservation of this fold among thiolases is illustrated in Figure 5 in which a Cα tracing of MVAS is aligned with other thiolases from bacteria, plants, and animals. The N-terminal domain also exhibits a rough internal symmetry with a 2-fold axis running between the two central helices. This symmetry is demonstrated in Figure 6, where the secondary structural elements of MVAS are displayed in a topology diagram. The red hash marks in this diagram denote the conserved residues illustrated in green in Figure 1 and are found to cluster on the loops between the major secondary structural elements, or on the large HMG-CoA synthase-specific insertions at the top left and right of the diagram (discussed below).

This symmetry within the N-terminal domain continues beyond the order of the secondary structural elements to the fine structure of the active site loop. This loop is identified by Cys111, the residue acetylated to form the enzyme−substrate complex prior to the condensation reaction (*16*), which is found at the tip of a β-turn between β-strand S3 and α-helix H3, located deep in the monomer and connected to the solvent by a long (18 Å) narrow tunnel. Examination of this active loop shows an unusual configuration of the

A

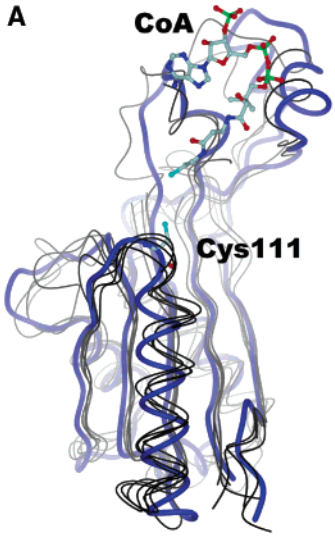

B

Name	PDB entry	residues in fold	residues aligned	RMSD	loops deleted	Aligned catalytic residues			
MVAS	1X9E	164	164	0	none	Cys 111	His 233	Asn 275	Glu 79
β-ketoacyl synthase	1HN9	168	151	1.5 Å	none	Cys 112	His 244	Asn 274	Thr 93
Chalcone synthase	1BQ6	143	131	1.7 Å	71-101 194-209	Cys 164	His 303	Asn 336	Thr 132
Peroxisomal thiolase	1AFW	138	116	1.8 Å	155-274	Cys 125	Asn 343	His 375	Val 93
Biosynthetic thiolase	1M4S	125	107	1.6 Å	none	Cys 89	Asn 316	His 348	Val 77

FIGURE 5: Alignment of MVAS with thiolase structures. (A) Cα tracing of the thiolase fold of MVAS and four examples of thiolase fold enzymes from the Protein Data Bank. The MVAS trace is in blue and follows the N-terminal half of the thiolase fold from residue 1 to 164. The aligned molecules are β-ketoacyl (ACP) synthase III from *E. coli* (EC 2.3.1.41), peroxisomal thiolase from *S. cerevisiae* (EC 2.3.1.16), biosynthetic thiolase from *Zoogloea ramigera* (EC 2.3.1.9), and chalcone synthase (EC 2.3.1.74) from alfalfa. The central α-helix (H3) is in the forefront of the figure, and the catalytic cysteine from MVAS is illustrated at the N-terminus of that helix. The orientation of the fold is chosen to roughly match that of the topology diagram in Figure 6. The coenzyme A binding region is illustrated with the CoA cocrystallized with chalcone synthase in PDB entry 1BQ6. This panel was constructed with DINO (http://www.dino3d.org) and rendered with PovRAY (http://www.povray.org). (B) Table indicating the structures aligned in panel A, the statistics of the alignments, and the residues aligned with the known catalytic residues of MVAS. The alignment was done in O, using the LSQ commands, as were the statistics (*33*). Note that peroxisomal thiolase (1AFW) and chalcone synthase (1BQ6) have large insertions intercalated between the secondary structural elements of the thiolase fold. These loops were not included in either the statistics or the illustration. It is striking to notice how the core catalytic residues for transferring the acyl group from the thio transfer molecule to the enzyme are conserved. The structural comparison shows that the positions of the histidine 233 and asparagine 275 equivalents are reversed in peroxisomal thiolase and biosynthetic thiolase vs that seen in MVAS. As the side chains of these residues form a rough equilateral triangle with the acylcysteine, this is not thought to represent a change in the fundamental chemistry. In addition, one notes the impressive nonconservation of Glu79, suggesting that it is important in the chemistry of the MVAS specific condensation reaction.

alanine residue just N-terminal to the cysteine that assumes an energetically unfavorable ϕ angle of 53° to accommodate the geometry of the turn. This unusual conformation is repeated in the topologically equivalent loop across the molecular pseudo-twofold axis, but with entirely different residues. This striking symmetry in both topology and detail between the halves of the N-terminal domain might suggest that it is the result of a gene duplication event. The structure of MVAS and the other thiolases demonstrate that molecular evolution has retained the structure and fold of the monomer halves while the primary amino acid sequence has clearly diverged, suggesting that the event occurred in the distant past.

C-Terminal Domain. The C-terminal domain (residues 320−383, seen in Figures 4 and 6) of MVAS is not a part of the classic thiolase fold but is a feature of the HMG-CoA synthase subfamily of thiolases. Comparison of the structure of MVAS to known thiolases suggests that the platonic thiolase fold ends at approximately residue 319 (Figure 6). A sequence alignment of representative HMG-CoA synthases (Figure 1) indicates that the C-terminal extension varies substantially in length. The shortest extensions, from 63 to 67 residues, are found in the prokaryotic synthases and the mitochondrial or "ketogenic" synthases of eukaryotic cells. The more extensive C-terminal extensions are approximately twice as long and are found in the cytoplasmic or "cholesterologenic" synthases of animal cells. The C-terminal domain of the synthases is of unknown function, as the shorter mitochondrial form is able to cover a null mutation of the more complex cytoplasmic form when overexpressed in Chinese hamster ovary cell culture (*39*). This leaves open the possibility that the C-terminal domain could be important for enzyme localization or post-translational activity control important in the whole animal, but not in cell culture.

Structure of the Active Site. As noted above, the active site loop of MVAS, like all the thiolases, is separated from the solvent by a long, narrow tunnel. The particular substrate specificity and chemistry of the different types of thiolases are controlled by large insertions between secondary structural elements of the thiolase fold (*40*, *41*) that provide specific functional residues and structures to the catalytic pocket at the bottom of this tunnel. MVAS does this as well, with the insertion between S1 and A1 (residues 13−50, Figure 6) providing the binding site for the adenine moiety of CoA and the symmetrically equivalent insertion between S′1 and A′1 (residues 181−197) contributing the catalytically important, synthase specific residues Asp184 and Phe185 to the catalytic pocket (discussed below). The actual access point for the CoA-bound ligands is an 18 Å deep tunnel as measured from the Cα of the acetylation site Cys111 at the bottom and the Cα of Ile37 located on the edge between the opening to the active site tunnel and solvent. Each monomer contains one active site, separated from the other monomer's active site by 23.5 Å, with the dimer arranged such that the active site tunnels are oriented away from one another. The outer edge of the active site tunnel nearest the solvent is populated by a number of basic residues (Lys32, -238, and -242) conserved in all HMG-CoA synthase sequences (Figure 1) and structurally paralleled in other members of the thiolase family.

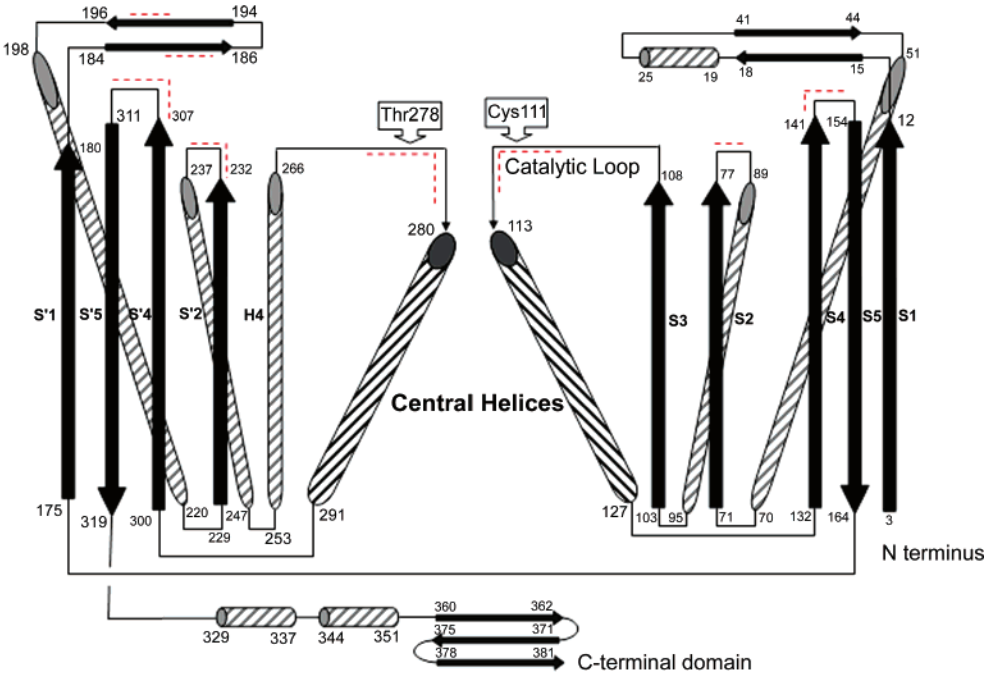

FIGURE 6: Topology of the MVAS monomer. This figure is a schematic of the major secondary structural elements of MVAS, illustrating the classic thiolase symmetry inherent in the topologic structure of the monomer. It is arranged as if the monomer was split between the central helices. If one reads from the inside out, the central helices are first, the β-sheets are outside of these, and the outer helices complete the domain. The symmetry of the topology implicitly makes the suggestion of a gene duplication as the origin of the monomer. The solid arrows represent β-strands, while the cylinders are α-helices. The red dashed lines point out amino acid sequence fragments that are conserved in HMG-CoA synthase across phyla, corresponding to the green blocks in the sequence alignment in Figure 1. The length of the object is roughly proportional to the length of the secondary structural elements, while the loop regions, for the sake of clarity, are not. The insertions (residues 13−50 and 181−197) containing the HMG-CoA synthase specific catalytic residues are seen at the top left and top right of the figure, and the synthase specific C-terminal domain is at the bottom.

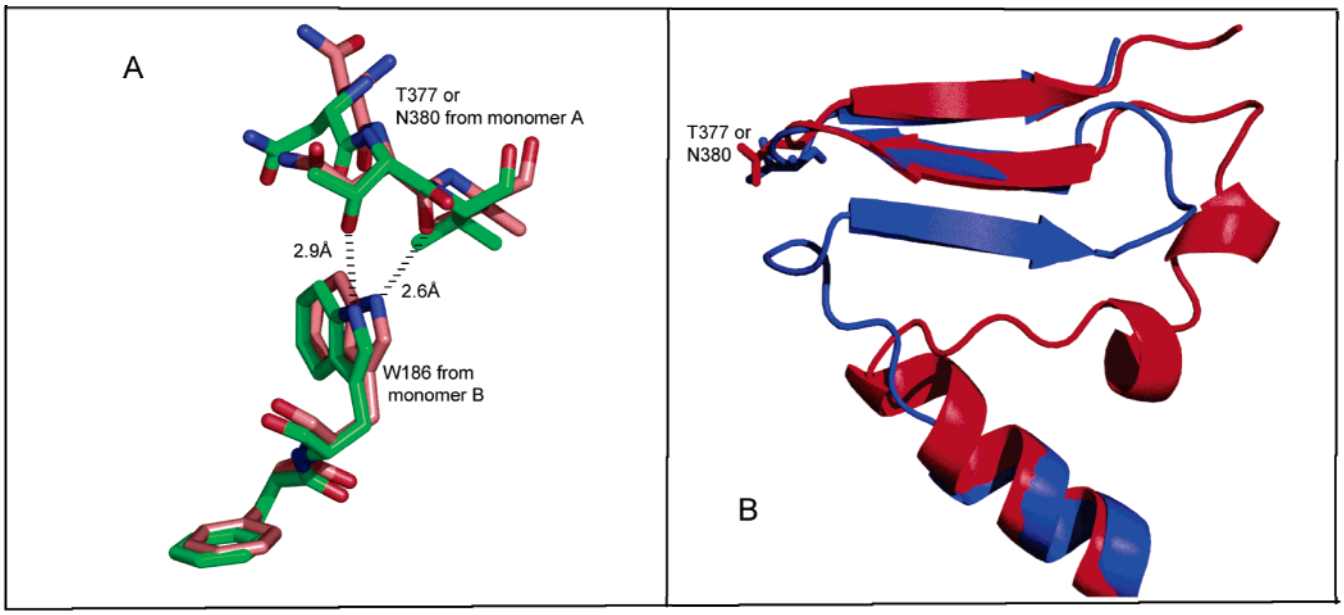

FIGURE 7: C-Terminal domain of HMG-CoA synthase from *E. faecalis* compared to that from *S. aureus*. The C-terminal residues from the structures were isolated and aligned with the equivalent residues from the *S. aureus* model (1TXT) (37) using the LSQ commands in O (*33*). In panel B, the ribbon cartoon of the *E. faecalis* structure is colored blue, demonstrating the additional β-strand, while that of *S. aureus* is colored red. Panel A is an expansion of the hydrogen bonding between the C-terminal domain of these two structures across the dimer interface to the adjacent monomer. It shows the bond between Thr377 (*E. faecalis* in green) or Asn380 (*S. aureus* in pink) and Trp186 of the other monomer. These aligned models were brought into PYMOL (http://pymol.sourceforge.net) where the figures were created.

At the deepest point of the active site tunnel is the β-turn containing Cys111 and a number of residues shown to be catalytically important in the avian enzyme, including His233, Glu79, Asp184, and Phe185 (Figure 8 and Table 1). These catalytic residues are partitioned onto two sides of the active site with residues His233 (3.6 Å from Cys 111) and Asn275 (5.4 Å) on one side of active cysteine. These two residues have been conserved across the entire family of synthetic and degradative thiolases (Figure 5B). Mutation of the cognate residue for His233 to Ala or Asn in the avian

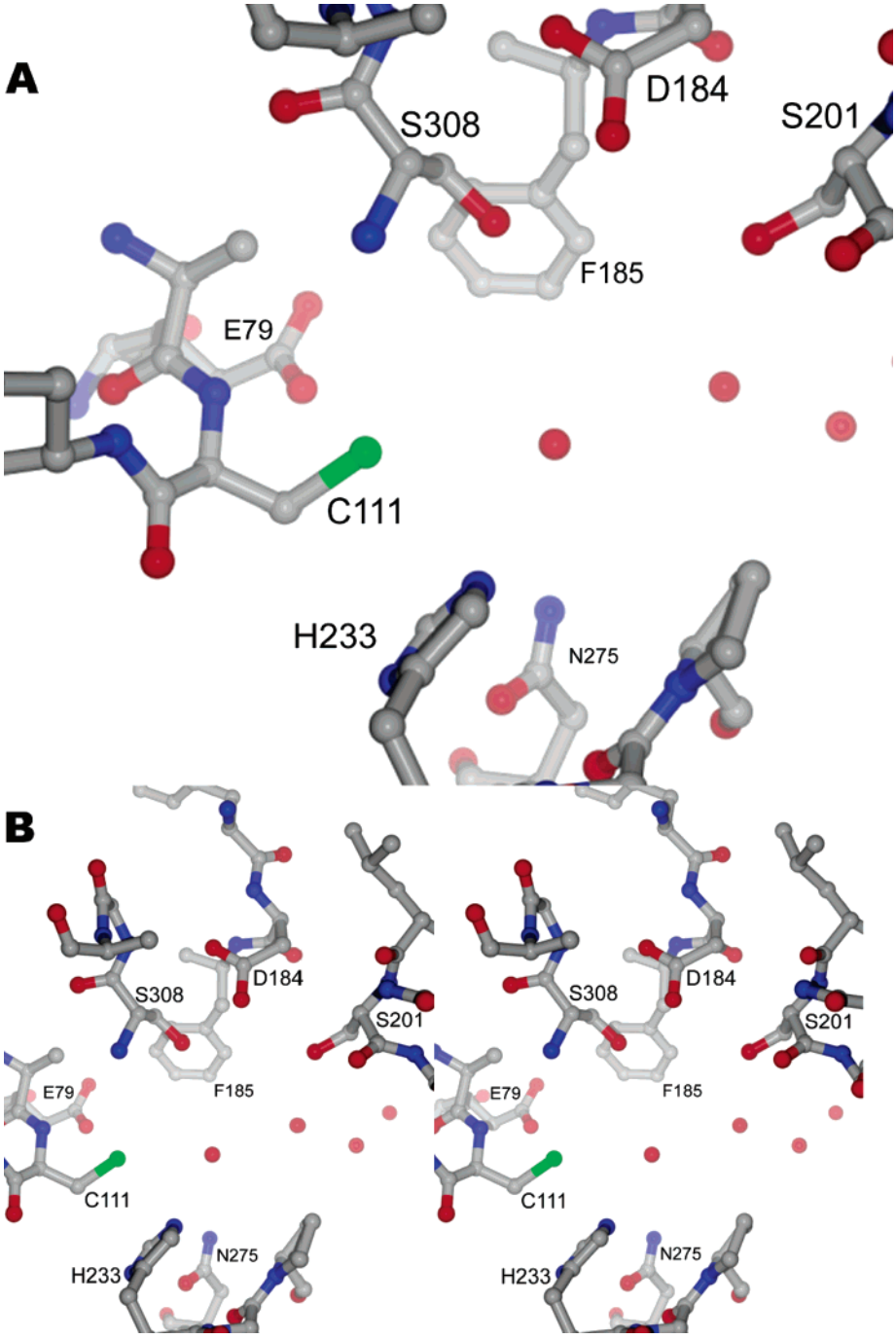

FIGURE 8: Catalytic residues in the active site of MVAS. (A) Arrangement of residues in the active site of MVAS. At the left is Cys111, the residue modified in the formation of the acyl−enzyme intermediate. Toward the bottom of the figure are residues His233 and Asn275. These residues are structurally conserved in all the thiolases aligned in Figure 6, and so are thought to be involved in the common chemistry of formation of the acyl−enzyme intermediate. In contrast, Glu79, Asp184, Phe185, and Ser201 and -308 are found on the opposite side of the active site. These residues are conserved in HMG-CoA synthases, but not in the general thiolase family. Because of this, these residues are thought to be involved in the unique chemistry of the HMG-CoA synthase condensation reaction of the acyl−enzyme intermediate with the acetoacetyl-CoA second substrate. (B) Same as panel A, but as a divergent stereoview to emphasize the three-dimensional arrangement of residues important for catalysis.

homologue diminishes activity, specifically in the initial formation of the acyl−enzyme thioester bond (*22*), while the effect of mutating Asn 275 has not yet been tested. The acyl−enzyme complex is a common intermediate in all the thiolases, and thus, the role of H233 is consistent with its universal conservation among these enzymes. This role is also consistent with its stabilization of the acetoacetyl−enzyme inhibitor complex, discussed below.

The Claisen condensation with the second ligand is the next step in the reaction mechanism of the biosynthetic thiolases. However, the carbon atom promoted to the nucleophilic carbanion is quite variable among these enzymes (*40*−*43*), resulting in their varied products. This variability is reflected in the remaining catalytic residues of the active site that are conserved within the HMG-CoA synthase family, but not in the other thiolases. These residues, Glu79, Asp184, Phe185, Ser201, and Ser308, are arrayed on the opposite side of the active site from His233 and Asn275 relative to Cys111 (Figure 8). A number of these residues have been studied with mutational analysis (Table 1), and all demon-

strate a decrease in enzyme activity when changed to an alanine. Glu79 is the closest residue of this group to Cys111 at 3.4 Å and is diametrically opposed to His233 (Figures 3 and 8). Mutation of Glu79 to alanine diminishes the overall activity of the enzyme by 5 orders of magnitude while demonstrating normal formation of the acyl−enzyme intermediate (*19*), thus firmly establishing it as a player in the synthase-specific condensation reaction (Rx3 in Figure 2). Ser308 has been assigned a primary role in the formation of an oxyanion hole that stabilizes the tetrahedral intermediate in this reaction (*37*). Mutations of other residues on this side of the active site with no clearly defined participation in the reaction also cause a decrease in overall activity, though their roles may be more structural than ones directly involved in catalysis.

A series of X-ray crystal structures of the staphylococcal HMG-CoA synthase have recently been published (*37*, *38*). An amino acid alignment shows these two bacterial enzymes are 60% identical, implying a close structural correlation. A superposition of the staphylococcal structure 1TXT on the native MVAS structure demonstrates an rmsd of the 380 Cα atoms of 0.8 Å over the entire molecule, with the primary differences occurring in the C-terminal domain. The overall structures show the same features, including the bridging 10-strand β-sheet and the extensive dimer interface. Hydrogen bonding networks and dimer interface contacts are generally preserved, though not necessarily with identical residues. The positions of residues in the active sites of the two native structures are virtually identical, although there is no evidence of oxidation of the active site cysteine in the *Enterococcus* MVAS.

The most striking structural difference between the structure of HMG-CoA synthase from *Enterococcus* and that of the enzyme from *Staphylococcus* is in the small C-terminal domain. In the two structures of MVAS from *Enterococcus* presented here, the C-terminal domain starts with two α-helices that extend along the outside of the five-layer globular structure and end in a tight three-stranded β-sheet. In contrast, all of the published staphylococcal crystal structures lack the first strand of the β-sheet, having instead a more extended loop structure (Figure 7B). In addition, the pattern of hydrogen bonding between the C-terminal β-sheet and Trp186 of the active site in the adjacent monomer is subtly different (Figure 7A). This observed variation in structure and hydrogen bonding pattern at the interface between the C-terminal domain and active site residues of the other monomer may express differences in the role this domain plays in the enzyme activity in the opposing monomer.

A timed sequence of staphylococcal structures has also been published showing an overlapping series of ligands in the active site as they evolve from the product, HMG-CoA, cocrystallized with the enzyme and trapped by the crystal contacts in the active site (*38*). Analysis of these structures assigns roles for the active site residues consistent with the phylogenetic analysis given above, but questions about the mechanism of the potent inhibition by the second substrate, acetoacetyl-CoA, still remain.

HMG-CoA Synthase in Complex with Acetoacetyl-CoA. To address the question of the mechanism of the potent inhibition by the second substrate, we have determined the structure of *Enterococcus* HMG-CoA synthase complexed with acetoacetyl-CoA. This ligand has a strong affinity for the active site of the native enzyme (K_m in the low micromolar range) of the native enzyme and inhibits the overall reaction when concentrations rise above the K_m (*14*, *15*). To avoid the problems with Cys111 oxidation present in the *S. aureus* acetoacetyl-CoA complex structure (1TXT) (*37*), our experimental protocol involved cocrystallizing acetoacetyl-CoA with the native protein purified over an affinity column followed by an extremely shallow gradient elution from a MonoQ anion exchange column and the aggressive use of reducing agents (see Methods).

The 1.9 Å crystal structure of acetoacetyl-CoA in complex with the *Enterococcus* enzyme shows density for the substrate in only one of the two active sites in the dimer, likely due to the crystal contact constraints at the opening of one of the active sites. In contrast to the results from the lower-resolution staphylococcal complex, this density clearly indicates that the thioester bond of the ligand has been broken and the acetoacetyl group attached to the enzyme. The reduced CoA molecule, freed of its acetoacetyl adduct, is in a position very similar to that found in these other MVAS binary structures with the adenine stabilized by Lys32 and the ribose phosphate hydrogen bonded to Lys242. From the interaction with the lysines on the surface, the CoA ligand adopts an extended conformation of the pantothenic acid portion for the ligand to interact with Cys111 at the bottom of the deep active site. A set of conserved hydrophobic residues (Tyr143, -205, -236, -277, and -306, Pro235, and Met239) populate the middle portion of the active site tunnel forming a hydrophobic lining. No direct hydrogen bonds are made between the enzyme and the CoA as it passes through this hydrophobic sleeve. Several of these residues have been mutated to leucine in the avian enzyme with only modest kinetic changes (Table 1), suggesting that only their general hydrophobic nature is important.

At the active site, the acetoacetyl group is found to have transferred from the CoA to a thioester bond with Cys111 making a covalent acetoacetyl−enzyme complex analogous to the acetyl−enzyme structure seen in the published staphylococcal binary structures (Figure 9). This is quite different from the published enzyme−acetoacetyl-CoA binary structures [PDB entries 1TXT (*37*), 1XPK, 1XPL, and 1XPM (*38*)] with the staphylococcal enzyme in which acetoacetyl-CoA is seen to remain intact in the active site barrel. The difference between these structures and the one presented here may be explained by the observation that the reactive cysteine in 1TXT was completely oxidized, thus precluding transfer of the acetoacetate. In the others, the nature of the experiment (trapping HMG-CoA in the active site and so forcing the energetically unfavorable reverse reaction) resulted in a mixture of molecular species in the active site with low partial occupancies.

In contrast to the acyl−enzyme complex seen in the staphylococcal structures in the database, the acetoacetyl group is oriented away from the residues thought to activate the acetate group for the condensation reaction. Specifically, the carbonyl of the published staphylococcal acyl−enzyme thioester bond is pointed toward the putative "thioanion hole" amide from Ser308 and the distal methyl group toward the base catalyst Glu79. In the acetoacetyl−enzyme structure presented here, the equivalent carbonyl is oriented 120° away

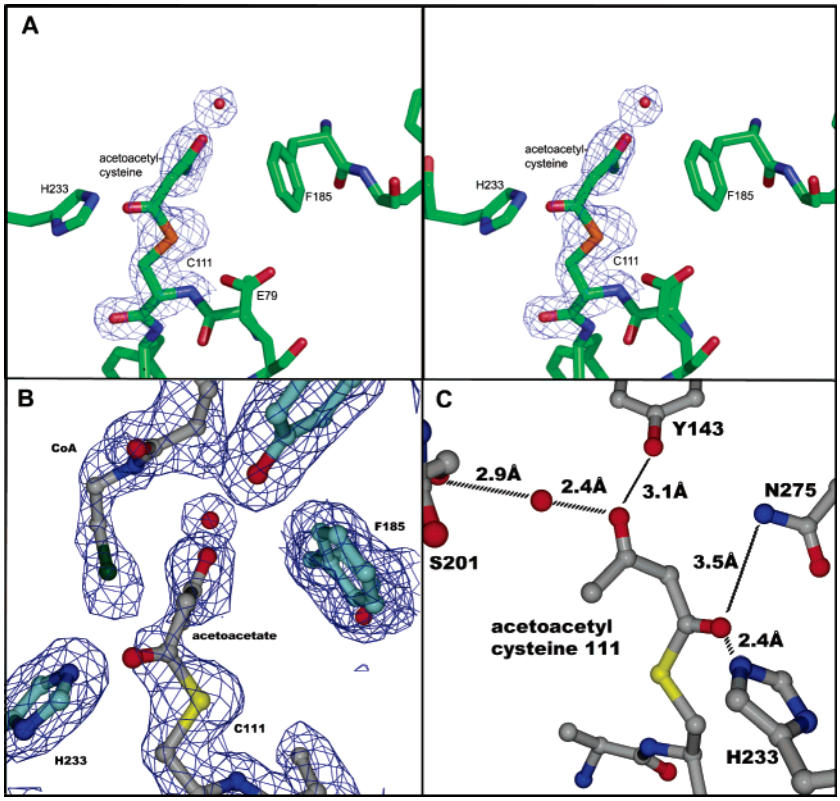

FIGURE 9: Covalent acetoacetyl-enzyme structure. (A) Divergent stereoview of the acetoacetyl ligand attached to the cysteine in the B monomer active site and the associated 1.0σ $2F_o - F_c$ density created in DINO (*45*). Also shown are catalytic residues His233, primarily involved in the initial formation of the aceto−enzyme complex, and Phe185, a catalytically essential residue. (B) A 1.0σ $2F_o - F_c$ electron density map covers the reduced CoA and Cys111 with the acetoacetate attached to it by a thioester bond. Again, His233 and Phe185 are shown. In panel C, the active site is rotated 120° about the acetoacetylcysteine axis. The pattern of hydrogen bonding to the conserved residues Tyr143, Asn175, Ser201, and His233 is illustrated, and the distances are marked.

from Ser308, making a close hydrogen bond (2.4 Å) to His233 and a more distant interaction (3.5 Å) with Asp275 (Figure 9B,C). The acetylacetyl−enzyme inhibitory species is further stabilized by the terminal carbonyl of the acetoacetylcysteine that makes a hydrogen bond to Tyr143 (3.1 Å) and is also stabilized by a water-mediated hydrogen bond to Ser201 (Figure 9C), both conserved active site residues of these enzymes. These hydrogen bonds serve to stabilize the acetoacetyl−enzyme complex and may also limit the subsequent hydrolysis or displacement by acetyl-CoA of the aceotacetate by making unavailable these catalytic amino acids. This would be consistent with the very low K_m acetoacetyl-CoA has for the reaction, and the profound inhibition seen when the concentration rises above the K_m (*14*).

An interesting observation of the inhibitory function of acetoacetyl-CoA came in a recent analysis of the HMG-CoA synthase from *Brassica junica* (*44*), where Nagegowda and co-workers found that the mutation of His188 to Asn, while diminishing the activity of the enzyme to 10% of that of the wild type, also eliminated the characteristic inhibition of acetoacetyl-CoA. This observation is remarkable in that the equivalent residue in the *Enterococcus* structure (Asp181) is not involved in the structure of the active site. But, while the particular residues are not conserved between *Brassica* and *Enterococcus*, the hydrogen bonding pattern connecting Asp181 to the active site loop on the adjacent monomer appears to be conserved, and directly stabilizes the ϕ angle of Ala110 (discussed above). The exact mechanism that would relieve the inhibition of the acetoacetyl−enzyme structure presented here awaits further study.

CONCLUSION

In summary, the X-ray crystal structure of HMG-CoA synthase from *E. faecalis* has been independently determined by MAD phasing to 2.4 Å resolution and the complex with the second substrate/inhibitor acetoacetyl-CoA to 1.9 Å. These structures reveal that the molecule has a characteristic thiolase fold whose internal symmetry suggests an ancient gene duplication event. The links between the catalytic site and the C-terminal β-sheet indicate the possibility of the modulation of enzyme activity through changes in this small domain. Comparisons to the recently published structure of the staphylococcal HMG-CoA synthase demonstrate substantial differences in structure and more subtle differences in interdomain hydrogen bonding in this domain. The active sites of the enterococcal and staphylococcal structures are structurally identical, and a phylogenetic analysis of the active site residues is consistent with the findings of trapped liganded structures. Finally, the structure of the enterococcal enzyme complexed with the second substrate/inhibitor acetoacetyl-CoA demonstrates that it forms a covalent acetoacetyl−enzyme complex that is stabilized by close hydrogen bonding to His233. This conformation of the acetoacetate group blocks subsequent hydrolysis by preventing activation of a solvent molecule and results in inhibition of HMG-CoA synthase activity.

ACKNOWLEDGMENT

We gratefully acknowledge the able and enthusiastic assistance provided by the staff of the Advanced Photon Source, beamlines 14ID and 17ID. Without the capabilities of this marvelous institution, this project would not have happened. Use of the Advanced Photon Source was supported by the U.S. Department of Energy, Basic Energy Sciences, Office of Science, under Contract W-31-109-Eng-38. Use of the BioCARS Sector 14 was supported by the National Institutes of Health, National Center for Research Resources, under Grant RR07707. Use of IMCA-CAT beamline 17-ID (or 17-BM) at the Advanced Photon Source was supported by the companies of the Industrial Macromolecular Crystallography Association through a contract with the Illinois Institute of Technology.

SUPPORTING INFORMATION AVAILABLE

An enlarged version of Figure 1, the amino acid alignment of members of the HMG-CoA synthase family. This material is available free of charge via the Internet at http://pubs.acs.org.

REFERENCES

1. Alberts, B., Bray, D., Lewis, J., Raff, M., Roberts, K., and Watson, J. D. (1989) *Molecular Biology of the Cell*, Garland Publishing, New York.
2. Lange, B. M., Rujan, T., Martin, W., and Croteau, R. (2000) Isoprenoid biosynthesis: The evolution of two ancient and distinct pathways across genomes, *Proc. Natl. Acad. Sci. U.S.A. 97*, 13172−13177.
3. Eisenreich, W., Schwarz, M., Cartayrade, A., Arigoni, D., Zenk, M. H., and Bacher, A. (1998) The deoxyxylulose phosphate pathway of terpenoid biosynthesis in plants and microorganisms, *Chem. Biol. 5*, R221−R233.
4. Huang, W., Jia, J., Edwards, P., Dehesh, K., Schneider, G., and Lindqvist, Y. (1998) Crystal structure of *β*-ketoacyl-acyl carrier protein synthase II from *E. coli* reveals the molecular architecture of condensing enzymes, *EMBO J. 17*, 1183−1191.
5. Mathieu, M., Zeelen, J. P., Pauptit, R. A., Erdmann, R., Kunau, W. H., and Wierenga, R. K. (1994) The 2.8-Angstrom crystal structure of peroxisomal 3-ketoacyl-CoA thiolase of *Saccharomyces cerevisiae*: A 5-layered α-*β*-α-*β*-α structure constructed from 2 core domains of identical topology, *Structure 2*, 797−808.
6. Sutherlin, A., Hedl, M., Sanchez-Neri, B., Burgner, J. W., Stauffacher, C. V., and Rodwell, V. W. (2002) *Enterococcus faecalis* 3-hydroxy-3-methylglutaryl coenzyme A synthase, an enzyme of isopentenyl diphosphate biosynthesis, *J. Bacteriol. 184*, 4065−4070.
7. Kattar-Cooley, P. A., Wang, H. H., Mende-Mueller, L. M., and Miziorko, H. M. (1990) Avian liver 3-hydroxy-3-methylglutaryl-CoA synthase: Distinct genes encode the cholesterogenic and ketogenic isozymes, *Arch. Biochem. Biophys. 283* (2), 523−531.
8. Gil, G., Brown, M. S., and Goldstein, J. L. (1986) Cytoplasmic 3-hydroxy-3-methylglutaryl coenzyme-A synthase from the hamster. II. Isolation of the gene and characterization of the 5′ flanking region, *J. Biol. Chem. 261*, 3717−3724.
9. Yokoyama, C., Wang, X. D., Briggs, M. R., Admon, A., Wu, J., Hua, X. X., Goldstein, J. L., and Brown, M. S. (1993) SREBP-1, a basic-helix-loop-helix-leucine zipper protein that controls transcription of the low-density-lipoprotein receptor gene, *Cell 75*, 187−197.
10. Gil-Gomez, G., Ayte, J., and Hegardt, F. G. (1993) The rat mitochondrial 3-hydroxy-3-methylglutaryl-coenzyme-A-synthase gene contains elements that mediate its multihormonal regulation and tissue specificity, *Eur. J. Biochem. 213*, 773−779.
11. Hegardt, F. G. (1999) Mitochondrial 3-hydroxy-3-methylglutaryl-CoA synthase: A control enzyme in ketogenesis, *Biochem. J. 338*, 569−582.
12. Rodriguez, J. C., Gilgomez, G., Hegardt, F. G., and Haron, D. (1994) Peroxisome proliferator-activated receptor mediates induction of the mitochondrial 3-hydroxy-3 methylglutaryl-coA synthase gene by fatty-acids, *J. Biol. Chem. 269*, 18767−18772.
13. Miziorko, H. M., and Lane, M. D. (1977) 3-Hydroxy-3-methylgutaryl-coA synthase. Participation of acetyl-S-enzyme and enzyme-S-hydroxymethylgutaryl-SCoA intermediates in the reaction, *J. Biol. Chem. 252*, 1414−1420.
14. Lowe, D. M., and Tubbs, P. K. (1985) 3-Hydroxy-3-methylglutaryl-coenzyme A synthase from ox liver. Purification, molecular and catalytic properties, *Biochem. J. 227*, 591−599.
15. Middleton, B. (1972) Kinetic mechanism of 3-hydroxy-3-methylglutaryl-coenzyme-A synthase from bakers yeast, *Biochem. J. 126*, 35−47.
16. Misra, I., Narasimhan, C., and Miziorko, H. M. (1993) Avian 3-hydroxy-3-methylglutaryl-coA synthase: Characterization of a recombinant cholesterogenic isozyme and demonstration of the requirement for a sulfhydryl functionality in formation of the acetyl-enzyme reaction intermediate, *J. Biol. Chem. 268*, 12129−12135.
17. Miziorko, H. M., and Behnke, C. E. (1985) Amino acid sequence of an active-site peptide of avian liver mitochondrial 3-hydroxy-3-methylglutaryl-coA synthase, *J. Biol. Chem. 260*, 3513−3516.
18. Miziorko, H. M., and Vinarov, D. A. (2002) Detection of covalent tetrahedral adducts by differential isotope shift C-13 NMR: Acetyl-enzyme reaction intermediate formed by 3-hydroxy-3-methylglutaryl-CoA synthase, *Methods Enzymol. 354*, 208−223.
19. Chun, K. Y., Vinarov, D. A., Zajicek, J., and Miziorko, H. M. (2000) 3-Hydroxy-3-methylglutaryl-CoA synthase: A role for glutamate 95 in general acid/base catalysis of C−C bond formation, *J. Biol. Chem. 275*, 17946−17953.
20. Chun, K. Y., Vinarov, D. A., and Miziorko, H. M. (2000) 3-Hydroxy-3-methylglutaryl-CoA synthase: Participation of invariant acidic residues in formation of the acetyl-S-enzyme reaction intermediate, *Biochemistry 39*, 14670−14681.
21. Wang, C. Z., Misra, I., and Miziorko, H. M. (2004) 3-Hydroxyl-3-methylglutaryl-CoA synthase: Utility of acetyldithio-CoA in detecting the influence of active site residues on substrate enolization, *J. Biol. Chem. 279* (39), 40283−40288
22. Misra, I., and Miziorko, H. M. (1996) Evidence for the interaction of avian 3-hydroxy-3-methylglutaryl-CoA synthase histidine 264 with acetoacetyl-CoA, *Biochemistry 35*, 9610−9616.
23. Misra, I., Wang, C. Z., and Miziorko, H. M. (2003) The influence of conserved aromatic residues in 3-hydroxy-3-methylglutaryl-CoA synthase, *J. Biol. Chem. 278*, 26443−26449.
24. Wilding, E. I., Kim, D. Y., Bryant, A. P., Gwynn, M. N., Lunsford, R. D., McDevitt, D., Myers, J. E., Jr., Rosenberg, M., Sylvester, D., Stauffacher, C. V., and Rodwell, V. W. (2000) Essentiality, expression, and characterization of the class II 3-hydroxy-3-methylglutaryl coenzyme A reductase of *Staphylococcus aureus*, *J. Bacteriol. 182*, 5147−5152.
25. Wilding, E. I., Brown, J. R., Bryant, A. P., Chalker, A. F., Holmes, D. J., Ingraham, K. A., Iordanescu, S., So, C. Y., Rosenberg, M., and Gwynn, M. N. (2000) Identification, evolution, and essentiality of the mevalonate pathway for isopentenyl diphosphate biosynthesis in Gram-positive cocci, *J. Bacteriol. 182*, 4319−4327.
26. Fridkin, S. K., Hageman, J. C., Morrison, M., Sanza, L. T., Como-Sabetti, K., Jernigan, J. A., Harriman, K., Harrison, L. H., Lynfield, R., and Farley, M. M. (2005) Methicillin-resistant *Staphylococcus aureus* disease in three communities, *N. Engl. J. Med. 352*, 1436−1444.
27. Doublie, S. (1997) Preparation of selenomethionyl protein for phase determination, *Methods Enzymol. 276*, 523−530.
28. Otwinowski, Z., and Minor, W. (1997) Processing of X-ray diffraction data collected in oscillation mode, *Methods Enzymol. 276*, 307−326.
29. Matthews, B. M. (1968) Solvent content of protein crystals, *J. Mol. Biol. 33*, 491−497.
30. Terwilliger, T. C., and Berendzen, J. (1997) Bayesian correlated MAD phasing, *Acta Crystallogr. D53*, 571−579.
31. Terwilliger, T. C. (1999) Reciprocal-space solvent flattening, *Acta Crystallogr. D55*, 1863−1871.
32. Terwilliger, T. C. (2003) Automated main-chain model building by template matching and iterative fragment extension, *Acta Crystallogr. 59*, 38−44.
33. Jones, T. A., Zou, J. Y., and Kjeldgaard, M. (1991) Improved methods for building protein models in electron-density and location of errors in these models, *Acta Crystallogr. A47*, 110−119.
34. Brunger, A. T., Adams, P. D., Clore, G. M., Delano, W. L., Gros, P., Grosse-Kunstleve, R. W., Jiang, J. S., Kuszewski, J., Nilges,

M., Pannu, N. S., Read, R. J., Rice, L. M., Simonson, T., and Warren, G. L. (1998) Crystallography & NMR system: A new software suite for macromolecular structure determination, *Acta Crystallogr. D54* (Part 5), 905−921.
35. Murshudov, G. N., Vagin, A. A., Lebedev, A., Wilson, K. S., and Dodson, E. J. (1999) Efficient anisotropic refinement of macromolecular structures using FFT, *Acta Crystallogr. D55* (Part 1), 247−255.
36. Collaborative Computational Project Number 4 (1999) The CCP4 Suite: Programs for protein crystallography, *Acta Crystallogr. D50*, 760−763.
37. Campobasso, N., Patel, M., Wilding, I. E., Kallender, H., Rosenberg, M., and Gwynn, M. N. (2004) *Staphylococcus aureus* 3-hydroxy-3-methylglutaryl-CoA synthase: Crystal structure and mechanism, *J. Biol. Chem. 279*, 44883−44888.
38. Theisen, M. J., Misra, I., Saadat, D., Campobasso, N., Miziorko, H. M., and Harrison, D. H. T. (2004) 3-Hydroxy-3-methylglutaryl-CoA synthase intermediate complex observed in "real-time", *Proc. Natl. Acad. Sci. U.S.A. 101*, 16442−16447.
39. Ortiz, J. A., Gil-Gomez, G., Casaroli-Marano, R. P., Vilaro, S., Hegardt, F. G., and Haro, D. (1994) Transfection of the ketogenic mitochondrial 3-hydroxy-3-methylglutaryl-coenzyme A synthase cDNA into Mev-1 cells corrects their auxotrophy for mevalonate, *J. Biol. Chem. 269*, 28523−28526.
40. Modis, Y., and Wierenga, R. K. (2000) Crystallographic analysis of the reaction pathway of *Zoogloea ramigera* biosynthetic thiolase, *J. Mol. Biol. 297*, 1171−1182.
41. Olsen, J. G., Kadziola, A., Wettstein-Knowles, P., Siggaard-Andersen, M., Lindquist, Y., and Larsen, S. (1999) The X-ray crystal structure of β-ketoacyl [acyl carrier protein] synthase I, *FEBS Lett. 460*, 46−52.
42. Ferrer, J. L., Jez, J. M., Bowman, M. E., Dixon, R. A., and Noel, J. P. (1999) Structure of chalcone synthase and the molecular basis of plant polyketide biosynthesis, *Nat. Struct. Biol. 6*, 775−784.
43. Kursula, P., Ojala, J., Lambeir, A. M., and Wierenga, R. K. (2002) The catalytic cycle of biosynthetic thiolase: A conformational journey of an acetyl group through four binding modes and two oxyanion holes, *Biochemistry 41*, 15543−15556.
44. Nagegowda, D. A., Bach, T. J., and Chye, M. L. (2004) *Brassica juncea* 3-hydroxy-3-methylglutaryl (HMG)-CoA synthase 1: Expression and characterization of recombinant wild-type and mutant enzymes, *Biochem. J. 383*, 517−527.
45. Kabsch, W., and Sander, C. (1983) Dictionary of protein secondary structure: Pattern recognition of hydrogen-bonded and geometrical features, *Biopolymers 12*, 2577−2637.

BI051487X